Chemical Geology 561 (2021) 120035

Contents lists available at ScienceDirect

Chemical Geology

journal homepage: www.elsevier.com/locate/chemgeo

Role of Fe- and Mn-(oxy)hydroxides on carbon and nutrient dynamics in agricultural soils: A chemical sequential extraction approach

Matthew Franks [a], Emily Duncan [b,c], Kevin King [b], Angélica Vázquez-Ortega [a,*]

[a] School of Earth, Environment and Society, Bowling Green State University, 190 Overman Hall, Bowling Green, OH 43403-0211, United States of America
[b] United States Department of Agriculture, Agricultural Research Service-Soil Drainage Research Unit, 590 Woody Hayes Drive, Columbus, OH 43210, United States of America
[c] Los Angeles Regional Water Quality Control Board, 320 W 4th St, Los Angeles, CA 91103, United States of America

ARTICLE INFO

Editor: B. Sherwood- Lollar

Keywords:
Soil nutrients
Soil organic carbon
Redox sensitive minerals
Soil health

ABSTRACT

Soil organic carbon (SOC) is a key component of maintaining favorable soil physical, biological and chemical health and ensures the sustainability of agricultural practices. Fe- and Mn-(oxy)hydroxide minerals play an important role in SOC stabilization and sequestration, as well as nutrient adsorption. To better understand the mineral phases responsible for the stabilization and sequestration of SOC, as well as PO_4^{-3} and NO_3^-; a four-step chemical sequential extraction (SE) was applied to soils from eight agricultural fields. Our SE scheme targeted operationally defined mineral phases namely, water extractable (Step 1), reductive dissolution of Mn-(oxy)hydroxide (Step 2), reductive dissolution of amorphous Fe-(oxy)hydroxide (Step 3), reductive dissolution of crystalline Fe-(oxy)hydroxide (Step 4) and residual minerals. Results showed that SOC was stabilized in the following order: crystalline Fe-(oxy)hydroxide > amorphous Fe-(oxy)hydroxide > Mn-(oxy)hydroxide. Fe- and Mn-(oxy)hydroxide minerals can promote the stabilization and long-term sequestration of SOC via the formation of inner sphere complexes (e.g., ligand-exchange) within the mineral surfaces contact zone. Fe- and Mn-(oxy)hydroxide minerals adsorbed PO_4^{-3} species to a large extent; however, NO_3^- was adsorbed marginally. Results indicated that PO_4^{-3} adsorption is largely mediated by Fe- and Mn-(oxy)hydroxide minerals, and NO_3^- by bulk soil organic matter. The coupling interaction between SOC, nutrients, and mineral phases in agricultural soils can better inform the application of conservation management practices to fully understand their effect on soil chemistry and health.

1. Introduction

Optimal content of soil organic carbon (SOC) increases nutrient retention, cation exchange capacity (CEC), porosity, and water holding capacity, decreases bulk density, and improves crop yields and profits for economical agriculture operations (Helling et al., 1964; Reeves, 1997; Sharpley et al., 2006; Turmel et al., 2015; Fink et al., 2016a; Moebius-Clune, 2016; Bünemann et al., 2018). For every 1 Mg ha^{-1} increase in the SOC pool within the rhizosphere, crop yields could be increased on average by 45 kg ha^{-1}, 30 kg ha^{-1}, and 165 kg ha^{-1} for wheat, rice, and maize, respectively (Lal, 2006). SOC is a key component for maintaining favorable soil physical, biological and chemical health. For instance, a large bioavailable cation pool will promote healthy and functional microbial, fungi, and plant communities (Moebius-Clune, 2016).

Research in the last decades have identified several mechanisms involved on SOC stabilization; for instance, physically stabilized by occlusion in microaggregates, organo-mineral complexes, and biochemically stabilized through the formation of recalcitrant organic compounds (e.g., humic substances) (Six et al., 2002). Al-, Fe-, Mn-(oxy) hydroxide minerals (e.g., gibbsite, ferrihydrite, goethite, MnO_2) play an important role in SOC stabilization (Lalonde et al., 2012; Allard et al., 2017). Understanding the mineral phases that are responsible for SOC stabilization in farm soils is an important aspect of soil health. The rate and extent of SOC mineralization depends on the soil organic matter (SOM) chemistry and its' interaction with Al-, Fe-, Mn-(oxy)hydroxide minerals, aluminosilicate clays, as well as soil microorganism's diversity and its metabolites (Oades, 1988). Vazquez-Ortega et al. (2014) reported high dissolved organic matter (DOM) sorption onto pristine Al- and Fe-(oxy)hydroxide minerals under continuous flow-through

* Corresponding author.
E-mail address: avazque@bgsu.edu (A. Vázquez-Ortega).

https://doi.org/10.1016/j.chemgeo.2020.120035
Received 24 July 2020; Received in revised form 15 December 2020; Accepted 17 December 2020
Available online 20 December 2020

conditions. Adsorption of organic compounds onto Al-, Fe-, Mn-(oxy) hydroxide and aluminosilicate clay minerals via cation bridging depend mainly on bioavailable cations, involving mainly calcium in neutral to alkaline soils and aluminum in acidic soils (Oades, 1988; Lützow et al., 2006). These interactions ensue aggregation of clay particles and organic compounds that aid in the soil structure stabilization (Oades, 1988). Other bonding mechanisms involved in SOM adsorption onto Al-, Fe-, Mn-(oxy)hydroxide minerals include anion exchange, ligand exchange–surface complexation, H bonding, van der Waals forces, and hydrophobic interactions (Eusterhues et al., 2005; von Lützow et al., 2006; Scheel et al., 2007; Joo et al., 2008). More generally, negatively charged organic matter functional groups (e.g., carboxyl and hydroxyl moieties) can interact with positively charged Al-, Fe-, Mn-(oxy)hydroxide minerals under adequate soil pH conditions; therefore, increasing SOM stabilization within the soil (Fink et al., 2016a).

Recent studies have discussed the effect of Al- and Fe-(oxy)hydroxide minerals on soil phosphorus (P) sorption capacities in agro-ecosystems (Bortoluzzi et al., 2015; Fink et al., 2016a, 2016b, 2016c). Bortoluzzi et al. (2015) showed that the maximum P adsorption capacity significantly correlated with the content of Fe-(oxy)hydroxide minerals (mainly goethite). Goethite exerts a disproportionate effect on P sorption because of its large specific surface area and the uniform spread of hydroxyl functional groups (≡Fe-OH) (Wei et al., 2014). Phosphate (PO_4^{3-}) bonds strongly with Fe-(oxy)hydroxide minerals via the formation of inner sphere complexes. PO_4^{3-} can form monodentate/mononuclear and bidentate/binuclear complexes with Fe-(oxy)hydroxide minerals (Essington, 2003; Sposito, 2008). The coupling interaction between SOC and Al-, Fe-, Mn-(oxy)hydroxide minerals can influence P adsorption in soils (Fink et al., 2016a). A tertiary complex can be formed between functional groups on the surface of Fe-(oxy)hydroxide minerals and organic compounds, and PO_4^{3-} species, favoring P sorption (Fink et al., 2016a). PO_4^{3-} forms a complex via cation bridging with the carboxyl functional group in the organic compound. Sorption experiments, using Al-, Fe-, Mn-(oxy)hydroxide minerals as sorbents, have also demonstrated that organic compounds can compete with PO_4^{3-} inhibiting P sorption (Hunt et al., 2007). We sought to evaluate the extent to which coupling interactions between SOC and Al-, Fe-, Mn-(oxy)hydroxide minerals influence PO_4^{3-} retention in agricultural soils. Knowledge on these interactions will inform nutrient management programs to effectively develop strategies suitable for specific crop rotations and soil types.

Agricultural best management practices (BMPs) are practical operation procedures that are effective in reducing the amount of nonpoint contamination and pollutants leaving an area where the BMPs are applied (EPA, 2020). The effect of BMPs (e.g., conservational tillage, cover crops, rotational crops, and 4R Nutrient Stewardship) on SOC has been emphasized in the previous decades of soil health research; however, the effect of BMPs on Fe- and Mn-(oxy)hydroxide mineral content in farm soils is not well understood (Kleinman et al., 2015; Sharpley et al., 2006; Smith et al., 2015). Conservation tillage enhances SOC stabilization and reduces carbon dioxide emission to the atmosphere (Hazarika et al., 2009). Inda et al. (2013) reported that when agricultural soils were managed under no-till for 21 years, the content of poorly crystalline iron oxides (e.g., ferrihydrite) increased in the soil surface when compared to conventional tillage. A more extensive understanding on the coupling interactions between SOC, redox sensitive minerals (e.g., Fe- and Mn-(oxy)hydroxide) and PO_4^{3-} in agricultural soils can better inform water management practices, such as drainage water management system (DWMS).

DWMS can potentially affect the content of Fe- and Mn-(oxy)hydroxide minerals in farm soils, with potential impacts on nutrient loss. A DWMS is an engineered control structure that is placed at the end of tile drainage outlets that carries subsurface tile water drainage away from agricultural fields. The DWMS has the capability of raising and lowering the outlet elevation by the installation of adjustable dams at the main tile outlet, which allows farmers to potentially hold water within the root zone. Advantages of DWMS include a reduction in tile discharge and reduced loads of nitrogen (N) and P (Williams et al., 2015). The reduced N and P loads are directly attributed to the decrease in discharge rate (Williams et al., 2015). Soil saturated conditions induced by the placement of DWMS can alter the soil pH, resulting in shifting redox conditions (Mansfeldt, 2004). Changes in soil pH and redox conditions can alter the soil's ability to retain or release organic matter and nutrients. For instance, saturated conditions (anoxic environment) can favor the reductive dissolution of Fe- and Mn-(oxy)hydroxide minerals in the subsoil, while unsaturated conditions would create oxic conditions. This shift in redox conditions will favor either the dissolution or precipitation of Fe- and Mn-(oxy)hydroxide minerals and in turn, associated SOM and nutrients will be dissolved in the soil solution or sorbed onto the surface of the Fe- and Mn-(oxy)hydroxide minerals (Thompson and Goyne, 2012).

Further research is needed to fully comprehend the coupling effect of SOC and Fe- and Mn-(oxy)hydroxide minerals on nutrient retention in farm soils. Understanding these biogeochemical processes will provide researchers and farmers with the basic knowledge needed to implement efficient strategies and manage BMPs to minimize nutrient loss into waterways and retain bioavailable nutrients for cash crops. Therefore, this study aimed to 1) identify operationally defined mineral phases (Fe- and Mn-(oxy)hydroxide minerals) and their associated SOC and P and N species via a chemical sequential extraction approach, and 2) correlate SOC content with N and P retention within each targeted operationally defined mineral phase. The sequential chemical extraction procedure was performed to quantify the mass fraction of SOC and PO_4^{3-} and NO_3^- associated with the water extractable, Mn-oxide, short range order Fe-oxide, long range order Fe-oxide, and residual minerals (Land et al., 1999; Laveuf et al., 2012).

2. Materials and methods

2.1. Study fields

Data from eight fields located in the Western Lake Erie watershed were identified and secured for this study. The fields are part of the USDA-ARS edge-of-field network and designed to quantify the effects of agricultural production and best management practices on soil and water quality (Williams et al., 2016). Fields 1, 2, 7, and 8 are located in shallow soils derived from wave-planed ground moraine and lake deposits overlaying Silurian aged carbonated bedrock (ODNR, 2006). Their soil series is Hoytville-Nappanee-Paulding-Toledo and these soils tends to be poorly drained (Table S1, Supplemental Information; USDA-NRCS, 2017). The remaining fields (3, 4, 5, and 6) are located in shallow soils composed mainly of lake deposits overlaying Mississippian aged sandstone, shale and siltstone bedrock (ODNR, 2006). Their soil series is Bennington-Cardington-Centerburg soil series and these soils tends to also be poorly drained (Table S1). Corn, soybean and wheat were produced on the fields using various degrees of tillage practices, including no till, conservational tillage and conventional tillage (Table S2, Supplemental Information; USDA- NRCS, 2017).

2.2. Sample collection and preparation

Soil cores were collected in the fall of 2017 at approximately one location for every two hectares (for example, eight sampling locations in a 16-ha field). At each sampling location five, one-meter deep cores (or depth of resistance) were collected. After collection, the cores were shipped to the USDA-ARS Soil Drainage Research Unit and stored at 4 °C until processing and analysis. Processing involved a 3-step procedure. First, the cores were divided into 0–5 cm, 5–15 cm, and 15–30 cm depths. Second, the five soil cores, that represented one location in a field were composited by depth. Therefore, any one sample is the composite of 5 soil cores of their corresponding depth. Samples were oven dried at 70 °C in paper bags, sieved through a 2 mm mesh,

pulverized using a Wiley Hammer Mill, and stored in Whirl-Pak bags. Upon receiving the samples at the Aqueous and Terrestrial Geochemistry Laboratory in Bowling Green State University, composited samples from each location in the fields were once again combined, resulting in one sample per field per depth (three samples per field or 24 total samples).

2.3. Sequential chemical extractions

Soil samples were subjected to a four-step sequential extraction (SE) scheme adapted from Land et al. (1999) and Laveuf et al. (2012) (Table 1). The extractions were performed on 1.0 g of dried soil samples placed individually in 50 mL polypropylene centrifuge tubes. Triplicate runs were made for each sample and the averaged results were used to yield calculations. After each extraction step, a rinse with nanopure water was conducted for 30 min with a 1:20 mass/volume ratio at room temperature. The nanopure water (18 MΩ) had a pH of 6.5. Extractions and rinses were performed under permanent shaking (100 rotations per minute). All extractions and rinses were centrifuged at 10,000 rpm (15,182 relative centrifugal force [RCF]) for 30 min to separate the supernatant and the residues and then filtered through a 0.45 μm nylon membrane. The rinses were then combined into the supernatant fraction. The soil residue was then subjected to the next extraction step, as described in Table 1. Blanks were also carried out in triplicate, following the same extraction scheme. The fractionation scheme (Table 1) resulted in five chemically distinct fractions, namely, water extractable (Step 1), reductive dissolution of Mn-(oxy)hydroxide, e.g., MnO_2 (Step 2), reductive dissolution of amorphous Fe-(oxy)hydroxide, e.g., ferrihydrite (Step 3), reductive dissolution of crystalline Fe-(oxy)hydroxide, e.g., goethite (Step 4), and the final residue fraction mainly consisting of resistant silicates and bulk SOM (Land et al., 1999; Laveuf et al., 2012).

2.4. Sample characterization

Major cations and metals (Fe, Mn, Al, Ca, K, Mg) from sequential extraction steps were determined using Inductively Coupled Plasma - Optical Emission Spectrometry (ICP-OES) (iCAP 6000 Series ICP Spectrometer, Thermo Electron Corporation) equipped with an ASX-520 AutoSampler. Samples were diluted using 5% nitric acid (ARISTAR®). The calibration curve was prepared using a Certipur-ICP mutli-element standard solution VIII, containing 24 elements (Al, B, Ba, Be, Bi, Ca, Cd, Co, Cr, Cu, Fe, Ga, K, Li, Mg, Mn, Na, Ni, Pb, Se, Sr, Te, Tl, and Zn) diluted in 10% nitric acid (ARISTAR®). Ground samples were loaded into standard sample holders and placed into a Panalytical X'Pert MPD diffractometer using Cu radiation at 45KV/40 mA for mineral phase characterization (H&M Analytical Services Company). The scans were run over the range of 3° to 80° with a step size of 0.0167° and an accumulated counting time of 250 s per step. Once the patterns had been collected, the crystalline phases were identified with the aid of the Powder Diffraction File published by the International Centre for Diffraction Data or the Inorganic Crystal Structure Database.

Total organic carbon (TOC) in the soil matrix was determined using high temperature oxidation followed by infrared detection of CO_2 (Shimadzu TOC-VCSH equipped with a solid sample module, SSM-5000A). The calibration curve was prepared using a soil certified reference material (Leco, 3.82% Carbon). TP in the soil matrix was determined using the alkaline persulfate digestion method followed by colorimetric detection using a Seal AQ2 Discrete Analyzer (Patton and Kryskalla, 2003). Briefly, one hundred mg of soil were suspended in 5 mL of ultrapure water and digested in 20 mL of potassium persulfate digestion reagent in a furnace at 121 °C for 1 h. A certified soil standard (SQC014-100G) was subjected to the same digestion procedure and the measured value was within 1% of the certified value. TN in the soil matrix was determined using USEPA 353.2 method, where nitrate (NO_3^-) was reduced by copperized cadmium to nitrite and measured spectrophotometrically at 520 nm. Dissolved organic carbon (DOC) in the extractions was determined using the carbon analyzer (Shimadzu TOC-VCSH) equipped with a liquid auto sampler (Shimadzu ASI-L). The calibration curve was prepared using an Organic Carbon Standard (RICCA, 2000 ppm). Phosphate (PO_4^{-3}) and NO_3^- in the extractions were determined by colorimetric methods using the Seal AQ2 Discrete Analyzer as well.

Table 1
Sequential Extraction steps 1–4 including targeted phases and procedures.

Step	Phases	Procedure
1	Water extractable	Nanopure water, 18 MΩ Adjust pH at 6.5 1:20 m/V 1 extraction, shake 1 h, room temperature
2	Mn-(oxy)hydroxides (e.g., Birnessite)	0.1 M $NH_2OH{\cdot}HCl$ in 0.1 M HCl Adjust pH at 2 1:20 m/V 1 extraction, shake 0.5 h, room temperature
3	Amorphous Fe-(oxy)hydroxides (e.g., Ferrihydrite)	0.25 M $NH_2OH{\cdot}HCl$ in 0.25 M HCl Adjust pH at 1.5 1:20 m/V 1 extraction, 2 h each, 60 °C
4	Crystalline Fe-(oxy)hydroxides (e.g., Goethite)	1.0 M $NH_2OH{\cdot}HCl$ in 1.0 M HCl Adjust pH at 1 1:20 m/V 1 extraction, 3 h, 90 °C

Adapted from Laveuf et al. (2012) and Land et al. (1999).

2.5. Data analysis

TOC, PO_4^{3-}, and NO_3^- concentrations (mg kg^{-1}) in each SE step were corrected by subtracting the respective concentrations from the blank samples. The corrected concentrations were multiplied by the volume generated at each extraction, then divided by the initial mass of soil used in each extraction. The mass fractions of TOC, PO_4^{3-}, and NO_3^- were determined by dividing the extracted concentrations between soil bulk total organic carbon, total phosphorous and total nitrogen, respectively. Correlation coefficients between TOC vs PO_4^{3-} and TOC vs NO_3^- from the sequential extraction steps were determined by the Pearson product-moment.

3. Results

3.1. Nutrient signatures in extractable pools

To explore the role of redox sensitive minerals (Fe- and Mn-(oxy) hydroxides) on the sorption of SOC, PO_4^{3-} and NO_3^-, mass fraction patterns were plotted for all SE steps (Figs. 1–3). These plots (discussed in order of SE steps, below) revealed that Fe- and Mn-(oxy)hydroxide minerals exert a substantial role on adsorbing PO_4^{3-} (Fig. 2). In contrast, NO_3^- was poorly retained by Fe- and Mn-(oxy)hydroxide minerals (Fig. 3). Total soil bulk TOC, TP, and TN and extractable mean TOC, PO_4^{3-}, and NO_3^- concentrations (mg kg^{-1}) as a function of depth for all studied fields are presented in Tables S3–S11 (Supplementary Information). Also, extracted Fe, Mn, Al, Ca, K, Mg concentrations (mg L^{-1}) are presented in Tables S12–S19 (Supplementary Information).

3.2. Water extractable TOC, PO_4^{3-}, and NO_3^- (step 1)

TOC, PO_4^{3-}, and NO_3^- adsorbed to positively charged soil particle surfaces that were water extractable at pH 6.5 (Table 1). Small TOC mass fractions ranging from 0.016 to 0.032 (Figs. 1 and 4A) were observed in the water extractable pool, among all fields and depths. The greatest water extractable TOC mass fractions were observed in Fields 1, 2, 7, and 8 (Fig. 4A). Fields 1 and 2 were managed under no till conditions and Fields 7 and 8 under conservation tillage (30% soil surface with crop

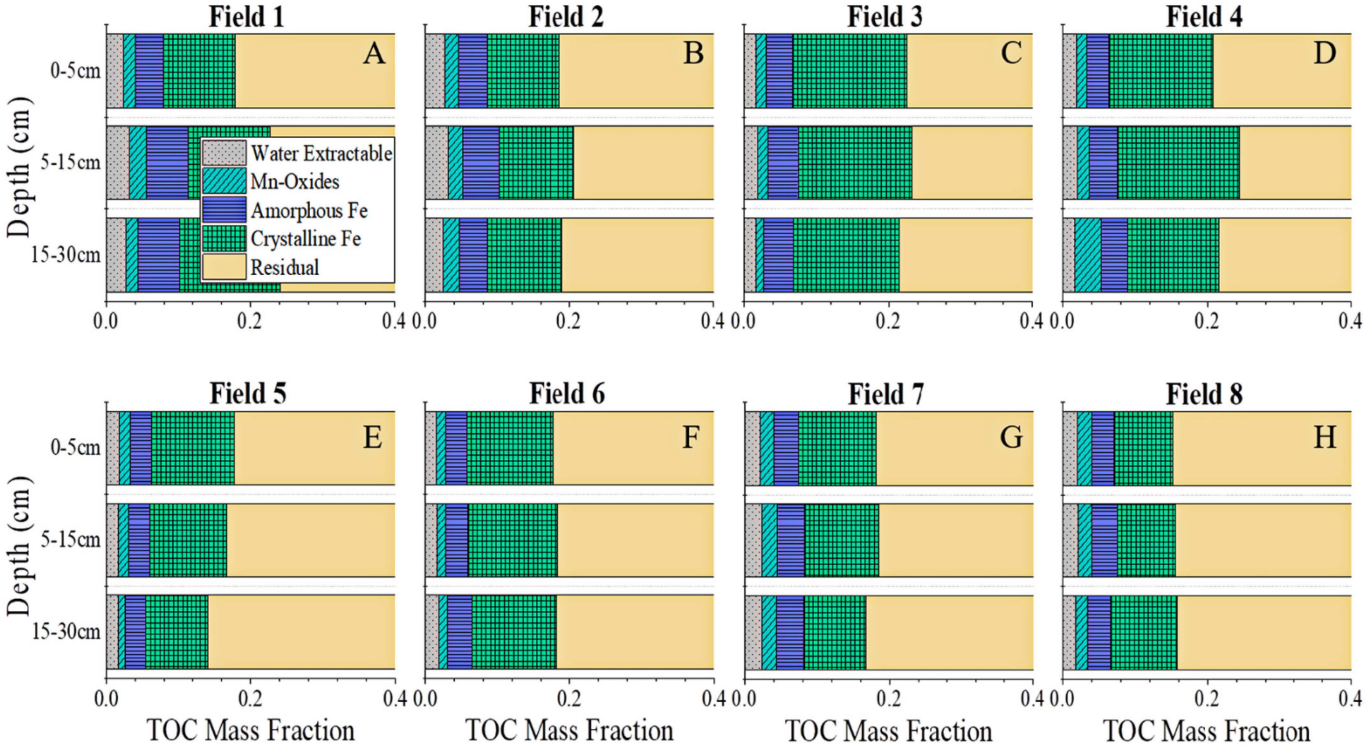

Fig. 1. Total organic carbon (TOC) mass fraction as a function of depth for all investigated fields. The mass fraction for this figure is scaled from 0.00–0.40.

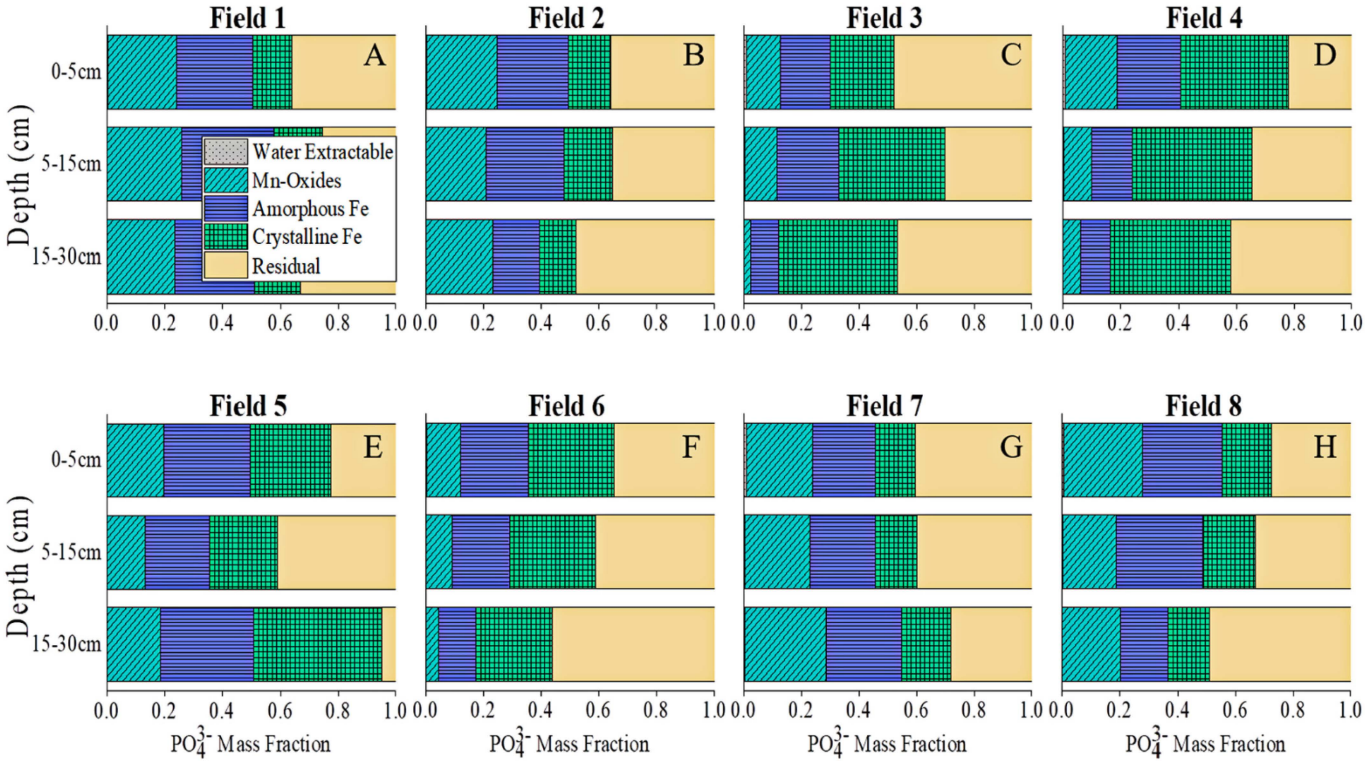

Fig. 2. Phosphate (PO_4^{3-}) mass fraction as a function of depth for all investigated fields. The mass fraction for this figure is scaled from 0.00–1.00.

residue). Among all fields and depths, the water extractable PO_4^{3-} mass fractions were barely noticeable, with values ranging from 0.00 to 0.009 (Fig. 2). No water extractable PO_4^{3-} mass fractions were observed in Fields 5 and 6, which were heavily tilled (6 times tilled over a 4-year period) (Fig. 4E). Small NO_3^- mass fractions were also observed in the water extractable pools, among all fields and depths, ranging from 0.001 to 0.016 (Fig. 3). The greatest water extractable NO_3^- mass fractions were observed in Fields 3 and 4 (6 times tilled over a 4-year period) (Fig. 4I). In the water extractable pools, positive correlations were observed between TOC vs PO_4^{3-} and TOC vs NO_3^- among all fields and

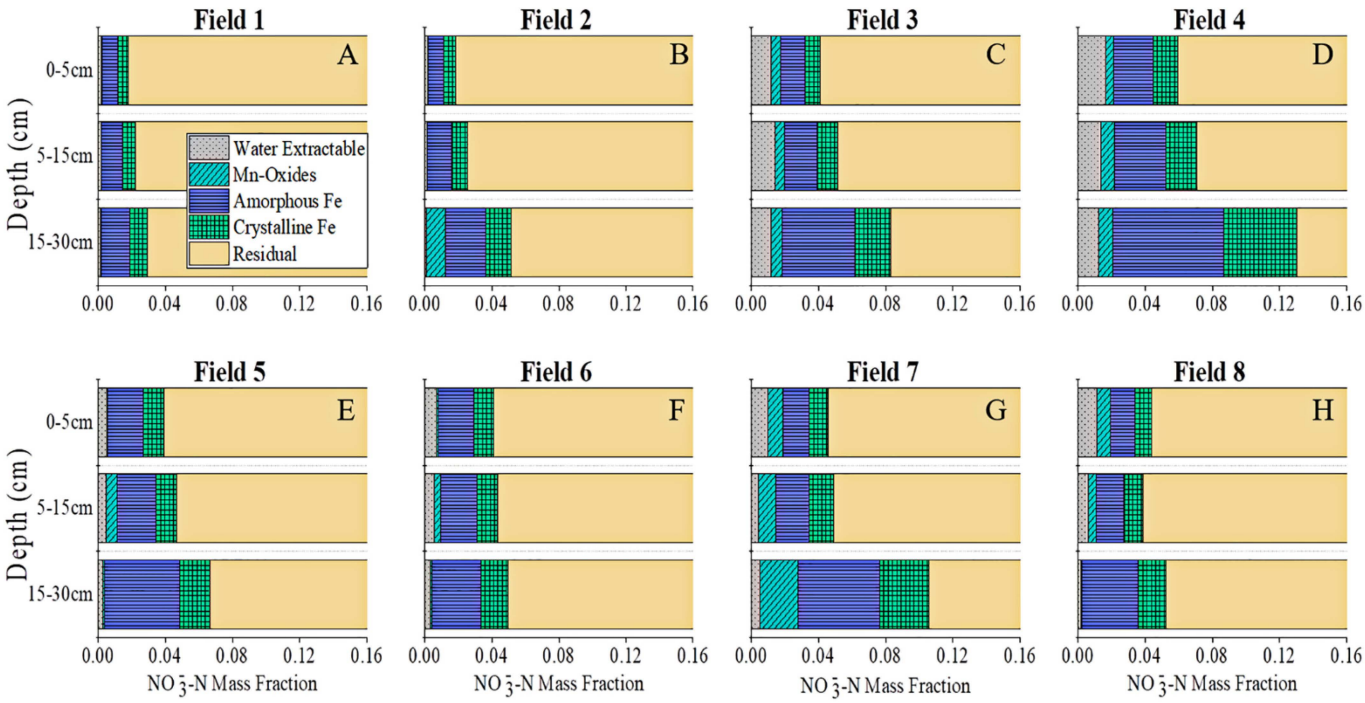

Fig. 3. Nitrate (NO_3-N) mass fraction as a function of depth for all investigated fields. The mass fraction for this figure is scaled from 0.00–0.16.

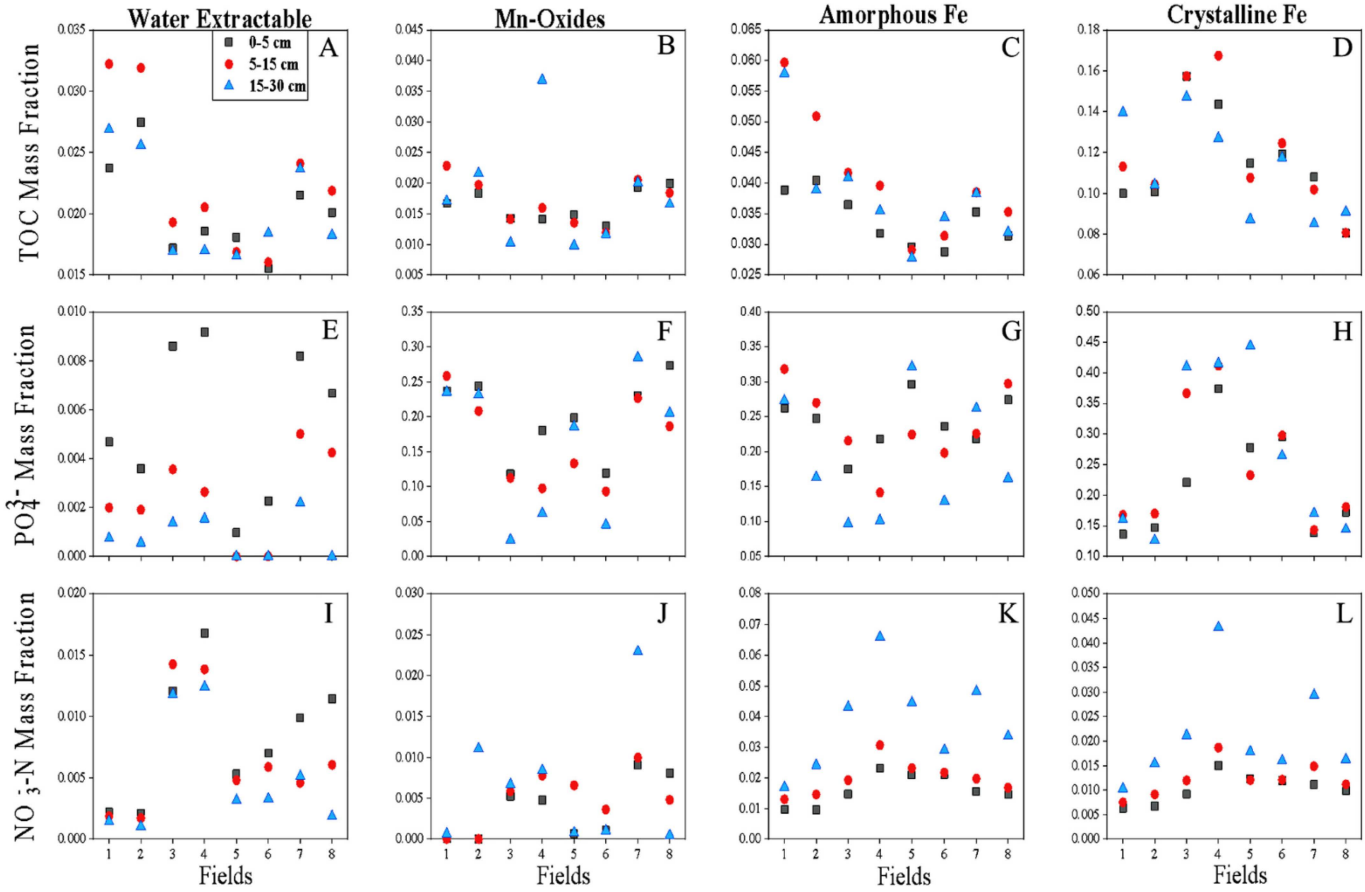

Fig. 4. Water extractable, Mn-oxides, amorphous Fe, and crystalline Fe mass fraction results for TOC, PO_4^{3-}, and NO_3^-N across all investigated fields as a function of depth. TOC mass fraction values range from 0.005–0.18 (A, B, C, D). PO_4^{3-} mass fraction values range from 0.00–0.50 (E, F, G, H). NO_3^-N mass fraction values range from 0.00–0.08 (I, J, K, L).

depths (p-value <0.05) (Tables 2 and 3).

3.3. Mn-(oxy)hydroxide-bound TOC, PO_4^{3-}, and NO_3^- (Step 2)

TOC, PO_4^{3-}, and NO_3^- adsorbed onto and/or co-precipitated within Mn-(oxy)hydroxide minerals that were dissolved under reductive conditions at pH 2 (Table 1). Mn-(oxy)hydroxide-bound TOC mass fractions, among all fields and depths, ranged from 0.012 to 0.037 (Figs. 1 and 4B). Overall, TOC mass fractions were relatively similar in all fields regardless of the tillage management practices, with the exception of Field 4 (Fig. 4B). PO_4^{3-} mass fractions associated with Mn-(oxy)hydroxide, among all fields and depths, ranged from 0.024 to 0.285 (Figs. 2 and 4F). In most fields, the Mn-(oxy)hydroxide-bound PO_4^{3-} mass fractions decreased as a function of depth. Overall, the greatest PO_4^{3-} mass fractions were observed in the fields managed under no till and conservation tillage (Fields 1, 2, 7, 8) (Fig. 4F). Small NO_3^- mass fractions were observed in the Mn-(oxy)hydroxide pools, among all fields and depths ranging from 0 to 0.023 (Fig. 3). The greatest Mn-(oxy)hydroxide-bound NO_3^- mass fractions were observed in Field 7 (8 times tilled with 30% biomass residue retention over a 4-year period) (Fig. 4J). In the Mn-(oxy)hydroxide pool, positive correlations were observed between TOC vs PO_4^{3-} (p-value < 0.05, except in Field 2) (Table 2). However, the association between TOC vs NO_3^- in the Mn-(oxy)hydroxide pool produced both positive and negative correlations (Table 3). For instance, strong positive correlations were observed in Fields 3 and 8 (p-value <0.05). In contrast, Fields 1, 2, and 4 exhibited strong negative correlations between TOC vs NO_3^- (p-value <0.05).

3.4. Amorphous Fe-(oxy)hydroxide-bound TOC, PO_4^{3-}, and NO_3^- (Step 3)

TOC, PO_4^{3-}, and NO_3^- adsorbed onto and/or co-precipitated within amorphous Fe-(oxy)hydroxide minerals that were dissolved under reductive conditions at pH 1.5 (Table 1). Amorphous Fe-(oxy)hydroxide-bound TOC mass fractions, among all fields and depths, ranged from 0.060 to 0.023 (Figs. 1 and 4C). The greatest TOC mass fractions were observed in Fields 1 and 2 at the bottom depths and with the least concentrations in Fields 5 and 6 (Fig. 4C). PO_4^{3-} mass fractions associated with amorphous Fe-(oxy)hydroxide, among all fields and depths, ranged from 0.100 to 0.321 (Figs. 2 and 4G). In most fields, the amorphous Fe-(oxy)hydroxide-bonded PO_4^{3-} mass fractions decreased as a function of depth. Small NO_3^- mass fractions were observed in the amorphous Fe-(oxy)hydroxide pool, among all fields and depths ranging from 0.010 to 0.066 (Fig. 3). The greatest amorphous Fe-(oxy)hydroxide-bonded NO_3^- mass fraction was observed in Field 4 (6 times tilled over a 4-year period) (Fig. 4K). In the amorphous Fe-(oxy)hydroxide pool, strong positive correlations were observed between TOC vs PO_4^{3-} (p-value < 0.05) (Table 2). However, the association between TOC vs NO_3^- in the amorphous Fe-(oxy)hydroxide pool produced negative correlations (p-value < 0.05) (Table 3).

Table 2
Correlation coefficients between TOC vs PO_4^{3-} (mg Kg^{-1}) for sequential extraction steps 1–4, for all fields.

Field ID	Water Extractable	Mn-Oxide	Amorphous Fe	Crystalline Fe
Field 1	0.89*	0.96*	0.94*	−0.44*
Field 2	0.99*	0.20	0.83*	0.48*
Field 3	0.90*	0.99*	0.99*	0.98*
Field 4	0.96*	0.51*	0.99*	0.98*
Field 5	0.83*	0.99*	0.99*	0.99*
Field 6	0.79*	0.99*	0.98*	0.99*
Field 7	0.98*	0.99*	0.99*	0.95*
Field 8	0.85*	0.15*	0.97*	0.67*

t-test, paired two sample for means, p-value (one tail), $\alpha = 0.05$.
* p-Value < 0.05.

Table 3
Correlation coefficients between TOC vs NO_3^- (mg Kg^{-1}) for sequential extraction steps 1–4, for all fields.

Field ID	Water extractable	Mn-Oxide	Amorphous Fe	Crystalline Fe
Field 1	0.99*	−0.91*	−0.15*	0.89*
Field 2	0.99*	−0.86	−0.99*	−0.88*
Field 3	0.97*	0.99*	−0.86*	−0.68*
Field 4	0.99*	−0.91*	−0.82*	−0.77*
Field 5	0.98*	0.20*	−0.95*	−0.37*
Field 6	0.99*	0.14*	−0.93*	−0.74*
Field 7	0.90*	−0.41*	−0.97*	−0.96*
Field 8	0.75*	0.97*	−0.95*	−0.93

t-Test, paired two sample for means, p-value (one tail), $\alpha = 0.05$.
* p-Value < 0.05.

3.5. Crystalline Fe-(oxy)hydroxide-bound TOC, PO_4^{3-}, and NO_3^- (Step 4)

TOC, PO_4^{3-}, and NO_3^- adsorbed onto and/or co-precipitated within crystalline Fe-(oxy)hydroxide minerals that were dissolved under reductive conditions at pH 1 (Table 1). Crystalline Fe-(oxy)hydroxide-bound TOC mass fractions, among all fields and depths, ranged from 0.081 to 0.167 (Figs. 1 and 4D). Among all redox sensitive minerals, the crystalline Fe-(oxy)hydroxide minerals adsorbed TOC to the greatest extent. The greatest TOC mass fractions were observed in Fields 3 and 4 at the middle depths and with the least concentrations in Field 8 (Fig. 4D). PO_4^{3-} mass fractions associated with crystalline Fe-(oxy)hydroxide, among all fields and depths, ranged from 0.126 to 0.444 (Figs. 2 and 4H). The greatest PO_4^{3-} mass fractions associated with the crystalline Fe-(oxy)hydroxide were observed in Fields 3, 4, and 5 (Fig. 4H). Small NO_3^- mass fractions were observed in the crystalline Fe-(oxy)hydroxide pool, among all fields and depths, ranging from 0.006 to 0.043 (Fig. 3). The greatest crystalline Fe-(oxy)hydroxide-bonded NO_3^- mass fraction was observed in Field 4 (6 times tilled over a 4-year period) (Fig. 4L). In the crystalline Fe-(oxy)hydroxide pool, strong positive correlations were observed between TOC vs PO_4^{3-}, with the exception of Field 1 (p-value <0.05) (Table 2). However, the association between TOC vs NO_3^- in the crystalline Fe-oxide pool produced negative correlations, with the exception of Field 1 (p-value <0.05) (Table 3).

3.6. Residual TOC, PO_4^{3-}, and NO_3^-

The residual pool includes resistant silicates (e.g., quartz, aluminosilicate clays), bulk SOM, as well as organo-metal colloids (Vázquez-Ortega et al., 2016). TOC adsorbed and/or occluded onto/between the aluminosilicate clay interlayers comprised the greatest mass fraction among all pools (Fig. 1). In most instances, residual-bound PO_4^{3-} mass fractions were the greatest at the 15–30 cm depth (Fig. 2). The least residual-bound PO_4^{3-} mass fraction was observed at the 15–30 cm depth in Field 5. The residual pool retained the greatest NO_3^- mass fractions when compared with all pools among all fields (Fig. 3).

4. Discussion

4.1. Role of Fe- and Mn-(oxy)hydroxide minerals on SOC stabilization

Based on our investigation, the operationally defined mineral phases stabilized SOC in the following order: crystalline Fe-(oxy)hydroxide > amorphous Fe-(oxy)hydroxide > Mn-(oxy)hydroxide (Figs. 1, and 4B-D). Our findings suggest that circa 20% of the SOC was directly bound to reactive Fe- and Mn-(oxy)hydroxides phases and these results are in agreement with Lalonde et al. (2012). Generally, within the Mn- and amorphous Fe-(oxy)hydroxide minerals, slightly high TOC mass fractions were observed in fields managed under conservation tillage (Fields 1, 2, 7, and 8) (Fig. 4B and C). Fields 1, 2, 7, and 8 contained the largest bulk SOC content as a function of depth when compared to fields managed under conventional tillage (Fields 3, 4, 5, and 6) (Table S3,

Supplemental Information). In addition, soils in Fields 1, 2, 7, and 8 belong to the same soil series: Hoytville series, which contain similar mineralogy composition and content (Soil Survey Staff, 2020; Figs. S1-S5, Supplemental Information). In contrast, Fields 3 and 4 displayed the largest TOC mass fraction within the crystalline Fe-(oxy)hydroxide phases (e.g., goethite). Studies have reported that soil organic compounds can inhibit the crystallization of Fe-(oxy)hydroxide minerals, in specific goethite (Schwertmann, 1966; Kodama and Schnitzer, 1977; Fink et al., 2016a, 2016b, 2016c). The conventional tilled fields contained the least bulk SOC content (Table S3, Supplemental Information) and this low SOC content could allowed for a larger proportion of goethite. The specific surface area (SSA) of ferrihydrite (a type of amorphous Fe-(oxy)hydroxide) can be as high of 400,000 m^2 Kg^{-1} (Schwertmann and Taylor, 1989) and for goethite it can range from 21,000 to 70,000 m^2 Kg^{-1} (Cornell and Schwertmann, 1996). When sorbed SOC (in mg Kg^{-1}, Tables S4-S11, Supplementary Information) was normalized by the minerals SSA (in m^2 Kg^{-1}, data not shown), SOC surface loadings for goethite were ca. 2–8 times larger than those for ferrihydrite. Our results are in agreement with Kaiser et al. (2007). Although, ferrihydrite has a larger SSA, goethite can exert a disproportional role on adsorbing SOC potentially due to larger abundance and the uniform spread of hydroxyl functional groups (≡Fe-OH) (Fink et al., 2016a; Wei et al., 2014). Fields 5 and 6 were also managed under conventional tillage; however, the TOC mass fraction was lower than in Fields 3 and 4. These cultivated fields belong to different soil series (Fields 3 and 4: Blount Series; Fields 5 and 6: Luray Series), potentially attributing to these sites different types and abundances of minerals (Soil Survey Staff, 2020).

Average soil pH values in all investigated fields as a function of depth ranged from 5.9 ± 0.5 to 7.1 ± 0.5 (Table 4). Soil pH values influence the surface charge of Fe- and Mn-(oxy)hydroxide minerals (Fink et al., 2016a; Wei et al., 2014). The point of zero charge (pzc) generally described the pH at which the net charge of a mineral surface is equal to zero (Sposito, 1998). Soil pH values below/above pzc indicate that the overall mineral surface is positively/negatively charged, respectively (Sposito, 1998). The typical pzc for MnO_2, ferrihydrite, and goethite are approximately 3.3, 8.5 and 8.0, respectively (Gray et al., 1978; Fink et al., 2016a). Under current soil pH conditions (at the time of collection), the overall surface charge of MnO_2 will be negatively charged. On the other hand, the overall surface charge of ferrihydrite and goethite will be mostly positively charged. Another parameter that provides insights into the interactions between SOM and Fe- and Mn-(oxy)hydroxide minerals, is the acidic dissociation constant (pK_a) of organic functional groups (e.g., carboxylic acid). The pK_a allows for prediction as to whether an acid will be predominantly dissociated or undissociated under given pH conditions (Turmel et al., 2015). The average soil pH values in all studied fields were above 5.86 (Table 4), which is greater than the typical pK_a for carboxylic acid (~4.5). At most soil pH conditions in our studied fields (at the time of soil collection), the carboxyl functional groups will be predominantly dissociated (Turmel et al., 2015). The negatively charged carboxyl moieties can be adsorbed onto the surface of Fe-(oxy)hydroxide minerals via the formation of ligand exchange–surface complexation (Eusterhues et al., 2005 and references within). The interactions between SOM with Fe-(oxy)hydroxide minerals can be described using the organo-mineral zonal model (Kleber et al., 2007). This conceptual model assumes the premise that SOM is a mixture of heterogeneous organic compounds, displaying amphiphilic moieties (hydrophilic and hydrophobic characteristics), and SOM is sorbed onto mineral phases in a discrete zonal sequence. The zones include the contact zone, hydrophobic zone, and kinetic zone, forming inner-sphere complexes (e.g., ligand exchange), van der Waals forces and cation bridging and hydrogen bonding, respectively (Kleber et al., 2007). SOM in the contact zone is less bioavailable due to strong covalent bonds; therefore, the exchange rate is low. SOM in the hydrophobic and kinetic zones exhibit moderate and high exchange rates, respectively. Fe- and Mn-(oxy)hydroxide minerals exert a strong role on SOC stabilization and bioavailability. Unless redox conditions favor the reductive dissolution of these minerals in the studied agricultural fields, SOM will be strongly sorbed allowing for a constant slow release of SOM as carbon and energy source for plants and microbial communities (Magdoff and Van Es, 2000).

Table 4
Average and standard deviation (SD) pH from 0 to 30 cm for all 8 investigated fields.

Field ID	Average pH	SD pH
Field 1	6.11	0.36
Field 2	5.86	0.45
Field 3	6.81	0.24
Field 4	7.09	0.47
Field 5	6.56	0.32
Field 6	6.62	0.46
Field 7	6.42	0.49
Field 8	6.43	0.37

4.2. *Coupling of Fe- and Mn-(oxy)hydroxides and soil organic matter on P and N sorption*

Operationally defined Fe- and Mn-(oxy)hydroxide mineral phases adsorbed PO_4^{-3} to a large extent in all investigated fields as a function of depth (Fig. 2). In Fields 1, 2, 7, and 8 (conservation tillage), Mn-(oxy)hydroxide mineral phases adsorbed a larger PO_4^{-3} mass fraction when compared to Fields 3, 4, 5, and 6 (conventional tillage) (Fig. 4F). In contrast, in Fields 3, 4, 5, and 6, crystalline Fe-(oxy)hydroxide minerals adsorbed PO_4^{-3} to a greater extent, when compared to Fields 1, 2, 7, and 8 (Fig. 4H). The high content of SOC in fields managed under conservation tillage can occupy the active sorption sites in the crystalline Fe-(oxy)hydroxide minerals hindering the PO_4^{-3} sorption (Hunt et al., 2007; Fink et al., 2016b). As stated in Section 4.1, SOC can inhibit the formation of crystalline Fe-(oxy)hydroxide mineral (e.g., goethite), further decreasing PO_4^{-3} sorption (Schwertmann, 1966; Kodama and Schnitzer, 1977). However, continuous tilling practices in Fields 3, 4, 5, and 6 will favor the decomposition of SOC (Balesdent et al., 2000), enhancing the neoformation of goethite and further promoting PO_4^{-3} sorption (Fink et al., 2016b).

Soil pH values in our studied fields, at the time of collection, will favor a net negative surface charge in the Mn-(oxy)hydroxide minerals, potentially adsorbing PO_4^{-3} via outer surface complexation (Mustafa et al., 2006). Cation bridging by alkaline earth cations (Ba^{2+}, Sr^{2+}, Ca^{2+}, Mg^{2+}) and transition metal ions (Mn^{2+}, Co^{2+}, Ni^{2+}) can enhance the sorption of PO_4^{-3} onto the surface of Mn-(oxy)hydroxide minerals (Kawashima et al., 1986). Fe-(oxy)hydroxide minerals would have an overall positive surface charge, augmenting PO_4^{-3} adsorption due to electrostatic attraction. PO_4^{-3} can form monodentate/mononuclear and bidentate/binuclear complexes with goethite surfaces (Fink et al., 2016a; Arai and Sparks, 2001; Belelli et al., 2014). These surface complexes result in no intercalated water molecules due to the strong formation of covalent bonds. The desorption and bioavailability of PO_4^{-3} depends on the binding energy of the complexes, with higher probability of PO_4^{-3} desorption in this sequence; binuclear > bidentate > monodentate complexes (Belelli et al., 2014). PO_4^{-3} bidentate/binuclear complexes desorb more readily because the P—O and Fe—P bond distances are longer (Belelli et al., 2014).

The formation of a tertiary complex between the hydroxyl group in the Fe-(oxy)hydroxide mineral surface, SOM, and PO_4^{-3} can enhance PO_4^{-3} sorption (Fink et al., 2016a). The electrostatic repulsion between the deprotonated carboxyl moiety and PO_4^{-3} is reduced by the intercalation of a cation, forming a cation bridging bond. SOM can also compete and desorb PO_4^{-3} from Fe-(oxy)hydroxide mineral surfaces (Fink et al., 2016a); however, our study showed strong positive correlations between TOC and PO_4^{-3} when the operationally defined Fe- and Mn-(oxy)hydroxide mineral phases underwent reductive dissolution (Table 2).

Overall, our results indicate that both SOM and Fe- and Mn-(oxy)hydroxide mineral phases are exerting a strong role on the retention of PO_4^{-3} in the studied farm soils, potentially controlling its desorption and bioavailability to plants and microorganisms.

The role of Fe- and Mn-(oxy)hydroxide mineral phases on nitrate (NO_3^-) sorption was considerably different to that of PO_4^{-3} (Table 3 and Figs. 3 and 4). NO_3^- was adsorbed marginally onto the surface of these minerals. Strong negative correlations were observed between TOC and NO_3^- when the operationally defined Fe- and Mn-(oxy)hydroxide mineral phases underwent reductive dissolution (Table 3), indicating that organic compounds were not facilitating NO_3^- sorption onto the surface of these minerals. However, strong positive correlations between bulk SOC and total N, as well as DOC and NO_3^- from the aqueous extraction were observed (data not shown), suggesting that sorption of nitrogen species in our studied soils is primarily control by bulk SOM.

5. Agricultural implications

SOM is a key component of maintaining favorable soil physical, biological and chemical health and ensures the sustainability of agricultural practices. Increasing SOM content increases nutrient retention, CEC, soil porosity, and water holding capacity, while it decreases bulk density, and improves crop yields (Helling et al., 1964; Reeves, 1997; Lal, 2006; Sharpley et al., 2006; Turmel et al., 2015; Fink et al., 2016a; Moebius-Clune, 2016; Bünemann et al., 2018). Additionally, an increased SOM content allows for anions, such as PO_4^{-3}, to be retained in soils at greater extent via the formation of outer surface complexation (Mustafa et al., 2006). It is important to understand the role of Fe- and Mn-(oxy)hydroxide minerals on SOM stabilization in agricultural soils to be able to manage them properly. Our study showed that Fe- and Mn-(oxy)hydroxide minerals sequestered SOC preferentially in the following order: crystalline Fe-(oxy)hydroxide > amorphous Fe-(oxy)hydroxide > Mn-(oxy)hydroxide. In fields managed under conservation tillage, the Mn-(oxy)hydroxide mineral pool adsorbed larger PO_4^{-3} mass fractions. In contrast, fields managed under conventional tillage, the crystalline Fe-(oxy)hydroxide minerals adsorbed PO_4^{-3} mass fractions to a greater extent. Finally, our results suggest the formation of tertiary complexes between the Fe-(oxy)hydroxide mineral surface, SOM, and PO_4^{-3}, as observed by the positive significant correlations in the extracted solutions from the reductive dissolution of Mn-(oxy)hydroxide, amorphous Fe-(oxy)hydroxide, and crystalline Fe-(oxy)hydroxide.

Furthermore, knowledge of the coupling interactions between Fe- and Mn-(oxy)hydroxide minerals, SOC, PO_4^{-3}, and soil pH, will allow for a deeper understanding and successful implementation of BMPs such as DWMS. Implementation of DWMS allows farmers to control the release of tile drainage water leaving their fields, reducing inputs of NO_3^- and PO_4^{-3} into receiving bodies. DWMS can alter redox conditions and soil pH under different water saturation conditions, potentially inducing the reductive dissolution of Fe- and Mn-(oxy)hydroxide minerals, ultimately affecting the adsorption/desorption of PO_4^{-3}. If desorption of PO_4^{-3} from Fe- and Mn-(oxy)hydroxide minerals were to happen and the DWMS is open, high concentrations of PO_4^{-3} would be released into receiving bodies, potentially exacerbating the effects that nutrients have on the growth of harmful algae blooms (Bullerjahn et al., 2016; Kane et al., 2014; Watson et al., 2016).

Declaration of Competing Interest

The authors declare that they have no known competing financial interests or personal relationships that could have appeared to influence the work reported in this paper.

Acknowledgements

This research was partially funded by the Building Strength Grant Programs - internal grants at Bowling Green State University (BGSU), BGSU Geology Foundation Fund and BGSU Center for Undergraduate Research and Scholarship. Special thanks to Lydia Archambo, Madison Brown, and Samuel Jefferson for their assistance on the analytical procedures and measurements.

Appendix A. Supplementary data

Supplementary data to this article can be found online at https://doi.org/10.1016/j.chemgeo.2020.120035.

References

Allard, S., Gutierrez, L., Fontaine, C., Croue, J., Gallard, H., 2017. Organic matter interactions with natural manganese oxide and synthetic birnessite. Sci. Total Environ. 583, 487–495.
Arai, Y., Sparks, D.L., 2001. ATR–FTIR spectroscopic investigation on phosphate adsorption mechanisms at the ferrihydrite–water interface. J. Colloid Interface Sci. 241, 317–326.
Balesdent, J., Chenu, C., Balabane, M., 2000. Relationship of soil organic matter dynamics to physical protection and tillage. Soil Tillage Res. 53, 215–230.
Belelli, P.G., Fuente, S.A., Castellani, N.J., 2014. Phosphate adsorption on goethite and Al-rich goethite. Comput. Mater. Sci. 85, 59–66.
Bortoluzzi, E.C., Pérez, C.A.S., Ardisson, J.D., Tiecher, T., Caner, L., 2015. Occurrence of iron and aluminum sesquioxides and their implications for the P sorption in subtropical soils. Appl. Clay Sci. 104, 196–204.
Bullerjahn, G.S., McKay, R.M., Davis, T.W., Baker, D.B., Boyer, G.L., D'Anglada, L.V., Doucette, G.J., Ho, J.C., Irwin, E.G., Kling, C.L., Kudela, R.M., Kurmayer, R., Michalak, A.M., Ortiz, J.D., Otten, T.G., Paerl, H.W., Qin, B., Sohngen, B.L., Stumpf, R.P., Visser, P.M., Wilhelm, S.W., 2016. Global solutions to regional problems: collecting global expertise to address the problem of harmful cyanobacterial blooms. A Lake Erie case study. Harmful Algae 54, 223–238.
Bünemann, E.K., Bongiorno, G., Bai, Z., Creamer, R.E., De Deyn, G., de Goede, R., Fleskens, L., Geissen, V., Kuyper, T.W., Mäder, P., Pulleman, M., Sukkel, W., van Groenigen, J.W., Brussaard, L., 2018. Soil quality – a critical review. Soil Biol. Biochem. 120, 105–125.
Cornell, R.M., Schwertmann, U., 1996. The Iron Oxides: Structure, Properties, Reactions, Occurrence, and Uses. VCH, Weinheim, New York.
EPA, 2020. United States Environmental Protection Agency. Watershed Academy Web. https://cfpub.epa.gov/watertrain/moduleFrame.cfm?parent_object_id=1362 (Accessed [06/22/2020]).
Essington, M.E., 2003. Soil and Water Chemistry: An Integrative Approach. CRC Press, Boca Raton (553 pp.).
Eusterhues, K., Rumpel, C., Kögel-Knabner, I., 2005. Organo-mineral associations in sandy acid forest soils: Importance of specific surface area, iron oxides and micropores. Eur. J. Soil Sci. 56, 753–763.
Fink, J.R., Inda, A.V., Tiecher, T., Barrón, V., 2016a. Iron oxides and organic matter on soil phosphorus availability. Cien. E Agrotecnol. 40, 369–379.
Fink, J.R., Inda, A.V., Bavaresco, J., Barrón, V., Torrent, J., Bayer, C., 2016b. Adsorption and desorption of phosphorus in subtropical soils as affected by management system and mineralogy. Soil Tillage Res. 155, 62–68.
Fink, J.R., Inda, A.V., Bavaresco, J., Sánchez-Rodríguez, A.R., Barrón, V., Torrent, J., Bayer, C., 2016c. Diffusion and uptake of phosphorus, and root development of corn seedlings, in three contrasting subtropical soils under conventional tillage or no-tillage. Biol. Fertil. Soils 52, 203–210.
Gray, M.J., Malati, M.A., Rophael, M.W., 1978. The point of zero charge of manganese dioxides. J. Electroanal. Chem. Interfacial Electrochem. 89, 135–140.
Hazarika, S., Parkinson, R., Bol, R., Dixon, L., Russell, P., Donovan, S., Allen, D., 2009. Effect of tillage system and straw management on organic matter dynamics. Agron. Sustain. Dev. 29 (4), 525–533.
Helling, C.S., Chesters, G., Corey, R.B., 1964. Contribution of organic matter and clay to soil cation-exchange capacity as affected by the pH of the saturating solution. Soil Sci. Soc. Am. J. 28, 517–520.
Hunt, J.F., Ohno, T., He, Z., Honeycutt, C.W., Dail, D.B., 2007. Inhibition of phosphorus sorption to goethite, gibbsite, and kaolin by fresh and decomposed organic matter. Biol. Fertil. Soils 44, 277–288.
Inda, A.V., Torrent, J., Barron, V., Bayer, C., Fink, J.R., 2013. Iron oxides dynamics in a subtropical Brazilian Paleudult under long-term no-tillage management. Sci. Agric. 70, 48–54.
Joo, J.C., Shackelford, C.D., Reardon, K.F., 2008. Association of humic acid with metal (hydr)oxide-coated sands at solid–water interfaces. J. Colloid Interface Sci. 317, 424–433.
Kaiser, K., Mikutta, R., Guggenberger, G., 2007. Increased stability of organic matter sorbed to ferrihydrite and goethite on aging. Soil Sci. Soc. Am. J. 71, 711–719.
Kane, D.D., Conroy, J.D., Peter Richards, R., Baker, D.B., Culver, D.A., 2014. Re-eutrophication of Lake Erie: correlations between tributary nutrient loads and phytoplankton biomass. J. Great Lakes Res. 40, 496–501.
Kawashima, M., Tainaka, Y., Hori, T., Koyama, M., Takamatsu, T., 1986. Phosphate adsorption onto hydrous manganese(IV) oxide in the presence of divalent cations. Water Res. 20, 471–475.
Kleber, M., Sollins, P., Sutton, R., 2007. A conceptual model of organo-mineral interactions in soils: Self-assembly of organic molecular fragments into zonal structures on mineral surfaces. Biogeochemistry 85, 9–24.

Kleinman, P.J.A., Smith, D.R., Bolster, C.H., Easton, Z.M., 2015. Phosphorus fate, management, and modeling in artificially drained systems. J. Environ. Qual. 44, 460–466.
Kodama, H., Schnitzer, M., 1977. Effect of fulvic acid on the crystallization of Fe (III) oxides. Geoderma 19 (4), 279–291.
Lal, R., 2006. Enhancing crop yields in the developing countries through restoration of the soil organic carbon pool in agricultural lands. L. Degrad. Dev. 17, 197–209.
Lalonde, K., Mucci, A., Ouellet, A., Gelinas, Y., 2012. Preservation of organic matter in sediments promoted by iron. Nature 483 (7388), 198–200.
Land, M., Ohlander, B., Ingri, J., Thunberg, J., 1999. Solid speciation and fractionation of rare earth elements in a spodosol profile from northern Sweden as revealed by sequential extraction. Chem. Geol. 160, 121–138.
Laveuf, C., Cornu, S., Guilherme, L.R.G., Guerin, A., Juillot, F., 2012. The impact of redox conditions on the rare earth element signature of redoximorphic features in a soil sequence developed from limestone. Geoderma 170, 25–38.
Lützow, M.V., Kögel-Knabner, I., Ekschmitt, K., Matzner, E., Guggenberger, G., Marschner, B., Flessa, H., 2006. Stabilization of organic matter in temperate soils: mechanisms and their relevance under different soil conditions - a review. Eur. J. Soil Sci. 57, 426–445.
Magdoff, F., Van Es, H., 2000. Building Soils for Better Crops (No. 631.584/M188b). Sustainable Agriculture Network, Beltsville.
Mansfeldt, T., 2004. Redox potential of bulk soil and soil solution concentration of nitrate, manganese, iron, and sulfate in two Gleysols. J. Plant Nutr. Soil Sci. 167 (1), 7–16.
Moebius-Clune, 2016. Comprehensive Assessment of Soil Health – The Cornell Framework, Edition 3.2. Cornell University, Geneva, NY.
Mustafa, S., Zaman, M.I., Khan, S., 2006. pH effect on phosphate sorption by crystalline MnO2. J. Colloid Interface Sci. 301, 370–375.
Oades, J.M., 1988. The retention of organic matter in soils. Biogeochemistry 5, 35–70.
ODNR, Ohio Division of Geological Survey, 2006. Bedrock Geologic Map of Ohio. Ohio Department of Natural Resources, Division of Geological Survey Map BG-1 (generalized page-size version with text, 2 p., scale 1:2,000,000. [Revised 2017.]).
Patton, C.J., Kryskalla, J.R., 2003. Methods of analysis by the US Geological Survey National Water Quality Laboratory: Evaluation of Alkaline Persulfate Digestion as an Alternative to Kjeldahl Digestion for Determination of Total and Dissolved Nitrogen and Phosphorus in Water, Vol. 3(4174). US Department of the Interior, US Geological Survey.
Reeves, D.W., 1997. The role of soil organic matter in maintaining soil quality in continuous cropping systems. Soil Tillage Res. 43, 131–167.
Scheel, T., Dörfler, C., Kalbitz, K., 2007. Precipitation of dissolved organic matter by aluminum stabilizes carbon in acidic forest soils. Soil Sci. Soc. Am. J. 71, 64–74.
Schwertmann, U., 1966. Inhibitory effect of soil organic matter on the crystallization of amorphous ferric hydroxide. Nature 212 (5062), 645–646.
Schwertmann, U., Taylor, R.M., 1989. Iron oxides. In: Dixon, J.B., Weed, S.B. (Eds.), Minerals in Soil Environments, 2 ed. Soil Science Society of America, Madison, pp. 379–438.
Sharpley, A.N., Daniel, T., Gibson, G., Bundy, L., Cabrera, M., Sims, T., Stevens, R., Lemunyon, J., Kleinman, P., Parry, R., 2006. Best Management Practices to Minimize Agricultural Phosphorus Impacts on Water Quality. United States Dep. Agric (ARS-163).
Six, J., Conant, R.T., Paul, E.A., Paustian, K., 2002. Stabilization mechanisms of soil organic matter: implications for C-saturation of soils. Plant Soil 241, 155–176.
Smith, D.R., Francesconi, W., Livingston, S.J., Huang, C., 2015. Phosphorus losses from monitored fields with conservation practices in the Lake Erie Basin, USA. Ambio 44, 319–331.
Soil Survey Staff, 2020. Natural Resources Conservation Service. United States Department of Agriculture. Web Soil Survey. Available online: http://websoilsurvey.sc.egov.usda.gov/ (Accessed [06/22/2020]).
Sposito, G., 1998. On points of zero charge. Environ. Sci. Technol. 32, 2815–2819.
Sposito, G., 2008. The Chemistry of Soils. Oxford University Press, New York, p. 321.
Thompson, A., Goyne, K.W., 2012. Introduction to the sorption of chemical constituents in soils. Nat. Educ. Knowledge 4 (4), 7.
Turmel, M.S., Speratti, A., Baudron, F., Verhulst, N., Govaerts, B., 2015. Crop residue management and soil health: a systems analysis. Agric. Syst. 134, 6–16.
USDA-NRCS, 2017. "Web Soil Survey." Web Soil Survey - Home. United States Department of Agriculture Natural Resources Conservation Service, 21 Aug. 2017. websoilsurvey.sc.egov.usda.gov/App/HomePage.htm.
Vazquez-Ortega, A., Hernandez-Ruiz, S., Amistadi, M.K., Rasmussen, C., Chorover, J., 2014. Fractionation of dissolved organic matter by (oxy)hydroxide-coated sands: competitive sorbate displacement during reactive transport. Vadose Zone J. 13 (7).
Vázquez-Ortega, A., Huckle, D., Perdrial, J., Amistadi, M.K., Durcik, M., Rasmussen, C., McIntosh, J., Chorover, J., 2016. Solid-phase redistribution of rare earth elements in hillslope pedons subjected to different hydrologic fluxes. Chem. Geol. 426, 1–18.
Watson, S.B., Miller, C., Arhonditsis, G., Boyer, G.L., Carmichael, W., Charlton, M.N., Confesor, R., Depew, D.C., Höök, T.O., Ludsin, S.A., Matisoff, G., McElmurry, S.P., Murray, M.W., Peter Richards, R., Rao, Y.R., Steffen, M.M., Wilhelm, S.W., 2016. The re-eutrophication of Lake Erie: harmful algal blooms and hypoxia. Harmful Algae 56, 44–66.
Wei, S.Y., Tan, W.F., Liu, F., Zhao, W., Weng, L.P., 2014. Surface properties and phosphate adsorption of binary systems containing goethite and kaolinite. Geoderma 213, 478–484.
Williams, M.R., King, K.W., Fausey, N.R., 2015. Drainage water management effects on tile discharge and water quality. Agric. Water Manag. 148, 43–51.
Williams, M.R., King, K.W., Ford, W., Fausey, N.R., 2016. Edge-of-field research to quantify the impacts of agricultural practices on water quality in Ohio. J. Soil Water Conserv. 71, 9A–12A.